A peer-reviewed version of this preprint was published in PeerJ on 23 December 2014.

View the peer-reviewed version (peerj.com/articles/716), which is the preferred citable publication unless you specifically need to cite this preprint.

Lamas LP, Main RP, Hutchinson JR. 2014. Ontogenetic scaling patterns and functional anatomy of the pelvic limb musculature in emus (*Dromaius novaehollandiae*) PeerJ 2:e716
https://doi.org/10.7717/peerj.716

Ontogenetic scaling patterns and functional anatomy of the pelvic limb musculature in emus (*Dromaius novaehollandiae*)

Luis P. Lamas[1*], Russell P. Main[2], John R. Hutchinson[1]

1. Structure and Motion Laboratory, Department of Comparative Biomedical Sciences, The Royal Veterinary College, Hawkshead Lane, Hatfield, AL9 7TA, United Kingdom.

2. *Department of Basic Medical Sciences, College of Veterinary Medicine, Purdue University, 625 Harrison Street, West Lafayette, IN 47907, USA.*

**L.P.Lamas is the Corresponding Author (llamas@rvc.ac.uk)*

Abstract

Emus (*Dromaius novaehollandiae*) are exclusively terrestrial, bipedal and cursorial ratites with some similar biomechanical characteristics to humans. Their growth rates are impressive as their body mass increases eighty-fold from hatching to adulthood whilst maintaining the same mode of locomotion throughout life. These ontogenetic characteristics stimulate biomechanical questions about the strategies that allow emus to cope with their rapid growth and locomotion, which can be partly addressed via scaling (allometric) analysis of morphology. In this study we have collected pelvic limb anatomical data (muscle architecture, tendon length, tendon mass and bone lengths) and calculated muscle physiological cross sectional area (PCSA) and average tendon cross sectional area from emus across three ontogenetic stages (n=17, body masses from 3.6 to 42 kg). The data were analysed by reduced major axis regression to determine how these biomechanically relevant aspects of morphology scaled with body mass. Muscle mass and PCSA showed a marked trend towards positive allometry (26 and 27 out of 34 muscles respectively) and fascicle length showed a more mixed scaling pattern. The long tendons of the main digital flexors scaled with positive allometry for all characteristics whilst other tendons demonstrated a less clear scaling pattern. Finally, the two longer bones of the limb (tibiotarsus and tarsometatarsus) also exhibited positive allometry for length and the two others (femur and first phalanx of digit III) had trends towards isometry. These results indicate that emus experience a relative increase in their muscle force-generating capacities, as well as potentially increasing the force-sustaining capacities of their tendons, as they grow. Furthermore, we have clarified anatomical descriptions and provided illustrations of the pelvic limb muscle-tendon units in emus.

PeerJ PrePrints

Introduction

Scaling studies (relating animal body mass to other biological parameters) have broadly elucidated locomotor adaptations across a wide range of body sizes. These studies have also described important size-related biomechanical (Alexander et al. 1979; Bertram & Biewener 1990; Biewener 1982; Gatesy & Biewener 1991; LaBarbera 1989; Maloiy et al. 1979; McMahon 1975) and metabolic (Gillooly et al. 2001; Hemmingsen 1960; Hokkanen 1986; Kleiber 1932; Schmidt-Nielsen 1984; Taylor et al. 1981) constraints across species. Intraspecific scaling studies are less common (Allen et al. 2010,2014; Carrier & Leon 1990; Carrier 1983; Dial & Jackson 2011; Main & Biewener 2007; Miller et al. 2008; Picasso 2012a; Smith & Wilson 2013; Young 2009, Picasso 2014) These ontogenetic approaches yield valuable insights into musculoskeletal adaptations to growth and potentially to identify size-related constraints on mechanical function within a species. Furthermore, studies of species where the mode of locomotion and basic anatomy remains similar during development contribute to the understanding of strategies and trade-offs that occur during growth. Such information can, for example, be used to comprehend developmental abnormalities and study intervention strategies to manage them.

Ratites are large flightless birds with cursorial morphology (e.g., Smith et al. 2010; Smith & Wilson 2013) that makes them attractive subjects for studies of terrestrial locomotion and bipedalism (Abourachid, 2000). Certain characteristics make emus (*Dromaius novaehollandiae*) particularly useful: they have some anatomical and functional similarities to other bipedal animals, including purportedly humans (Goetz et al. 2008). Compared to ostriches, they are generally easier to handle and train in experimental settings due to their smaller size and calmer temperament. Finally, their growth rate is impressive, as they multiply their body weight ~80 times in the first 18 months of life (Minnaar & Minnaar 1998) whilst maintaining the same cursorial mode of locomotion. Despite this interest there are still some discrepancies in published anatomical descriptions and depictions of the pelvic limb musculature of emus (Haughton 1867; Patak & Baldwin 1998; Vanden Berge & Zweers 1993), and clear visual anatomical aids are lacking in the literature.

Some of the biomechanical changes in the hindlimb occurring during the growth in emus have been described . Main and Biewener (2007) measured the skeletal strain patterns on the surfaces of the femur and the tibiotarsus (TBT) in running emus, demonstrating a significant increase in the magnitude of cranial and caudal femoral and caudal tibiotarsal strains during ontogeny, despite the enlargement and strengthening of those bones via positive allometric scaling of the second moment of area. Muscles have been shown to influence the strain patterns of bones (Yoshikawa et al. 1994), and although other factors are likely to be involved in the changes in peak bone strains reported across ontogeny (Main & Biewener 2007), allometric scaling of the musculature could also play a role in these differences in bone tissue loading. The strains induced by muscle contraction will be proportional to the muscle forces acting on the bone; therefore by estimating muscle forces (e.g., maximal force capacity based upon anatomy), associations between these two findings would be possible.

In order to build on already available biomechanical data for emus (Goetz et al. 2008; Main & Biewener 2007), we aim here to quantify the ontogenetic scaling patterns of four pelvic limb bones, pelvic limb muscles and their tendons and in the process describe and compare the functional and descriptive anatomy of the pelvic limb musculature of emus. We use regression analysis to determine the relationship of muscle architectural properties with body mass in an ontogenetic series of emus and then examine the implications of these findings for the locomotor ontogeny of emus, other ratites as well as extinct theropod dinosaurs.

Materials and methods

Animal subjects and care: UK group

We dissected 17 emus for this study, obtained from our ongoing research examining emu ontogenetic biomechanics (conducted with ethical approval under a UK Home Office license). The emus were divided in three groups of animals according to their age: Group 1: Five individuals at 4-6 weeks old; Group 2: Six 24-28 weeks (6 months) old individuals; and Group 3: Six 64-68 weeks (16 months) old individuals. All birds had been used as experimental animals and kept in a small pen (7x7m) for the first six weeks of life, after which they were moved to an outdoor larger enclosure with grass footing (40mx15m) until they were six months old; after this they were moved to a large (1.6 hectares) grass field (maximal animal density at one time was 8 birds/ha). The birds were all born in three consecutive yearly breeding seasons. Only the birds in Group 3 were from the same breeding season but not necessarily the same progenitors; birds from the other two Groups were from two different seasons.

All animals were hatched at a commercial breeding farm in the UK and raised from four weeks of age at the Royal Veterinary College. They were fed a commercial ostrich pelleted diet supplemented with grass and from six weeks of age were kept with free access to commercial food and grass. At 24 weeks, their diet changed from an ostrich grower diet to adult ostrich pelleted food (Dodson and Horrel Ltd., Kettering, Northamptonshire, UK). There were no restrictions or enforcements on the animals' regular exercise regime and all animals were allowed the same area and conditions to exercise during their development. All animals were euthanized after other experimental procedures were completed, by lethal intravenous injection of a barbiturate following induction of deep terminal general anaesthesia by intramuscular injection of ketamine and xylazine. Carcasses were kept frozen in a -20°C freezer for up to 2 years before dissection. Thawing was allowed at variable ambient temperatures and for variable amounts of time depending on the size of the animal, and dissection started no longer than 4 days after removal from the freezer. All dissections were performed within a six week period and led by the same individual (L.P.L.).

USA group of emus

Unpublished raw data of muscle masses from a different group of 29 emus (0.74 to 51.7 kg body mass) used for similar purposes as those described for the UK group were also included in this study. This group was bred and reared in the USA (Concord Field Station, Harvard University) under the care of another investigator (R.P.M.) who led all dissections for this group. The size and age composition for this group was more heterogeneous, and only body masses and muscle masses were available for analysis. Because the purpose of the dissections in the group was not a systematic ontogenetic musculoskeletal scaling study, the number of muscles dissected per animal varied.

Bone measurements

Maximal interarticular lengths of the femur, tibiotarsus (TBT), tarsometatarsus (TMT) and first phalanx of the middle (third) digit were measured using an ordinary flexible measuring tape (±1mm) once they were cleared of all soft tissues.

Myology and muscle architecture

We identified muscles of emus using four separate literature sources (Haughton 1867; Patak & Baldwin 1998; Smith et al. 2007; Vanden Berge & Zweers 1993); when our observations differed from these, we described the anatomical landmarks and attachments in detail according to our observations. General main actions of the muscle were defined based on these publications and confirmed by identifying the muscle attachments and paths and then mimicking the muscle action by applying tension on the muscle during dissection. We used additional reference to a biomechanical model of an ostrich (Hutchinson et al. 2014) to refine the three-dimensional actions of the hip muscles, as those actions are difficult to accurately ascertain from visual inspection and manipulation. Table 1 shows our simplified description of the anatomy, abbreviations used

PeerJ PrePrints

throughout this study, and inferred muscle actions. Figures 1 to 3 show schematic anatomical representations of the muscle anatomy.

To avoid freeze drying of the carcasses, we ensured all animals were frozen soon after euthanasia kept in sealed bags, and were not thawed and refrozen before dissection. The carcasses showed minimal autolysis and therefore an easier and better dissection during which muscle actions could be approximated without damaging their structure and attachments.

Dissection of the right pelvic limb muscles was performed in all specimens apart from the first two subjects in the 4-6 week old group, in which the muscles of the left limb were dissected first to standardise the technique. Measurements taken from the muscles of the left limb were not used (avoiding duplication of information), with the exception of when there were unidentified/damaged muscles from the right limb of the same specimen, in order to create a complete set of muscles for each specimen.

After identification of each muscle, we performed complete dissection and removal of it by transection at its origin and insertion(s). Next, the muscle was laid flat on a table and we took four muscle architectural measurements in a standard protocol: muscle mass (M_m), fascicle length (L_f), muscle belly length and pennation angle (Θ). Muscle mass was measured on an electronic scale (± 0.01 g) after removal of tendons, fat and aponeuroses. Fascicle length was measured from at least five random sites within the muscle belly using digital callipers (± 0.1 mm).Muscle belly length was measured as the length (± 1 mm) from the origin of the most proximal muscle fascicles to the insertion of the most distal fascicles into the distal tendon or aponeurosis. The pennation angle was measured at least five times using a goniometer (±5°) with the mean of the latter measurements was taken as the pennation angle for the muscle. The repeated measurements were taken from multiple cuts into the muscle to expose different anatomical orientations of the fascicles with the same muscle. This methodology minimises the differences that may be seen across an individual muscle and ensures mean values used for further calculations are representative of the overall architecture of the muscle. We calculated total limb muscle mass by adding the individual masses of the muscle bellies. Our approach was straightforward for most muscles, apart from three smaller muscles of the limb: IFI, ISF and FPPDII (Table 1), where minor dissection mistakes might have impaired estimates of their masses and architectural properties.

Muscle volume was calculated by dividing muscle mass by estimated muscle density of vertebrates (1.06 g cm^{-3}; (Brown et al. 2003; Hutchinson et al. 2014; Mendez & Keys 1960)). From these data we calculated physiological cross-sectional area (PCSA) for each muscle via the standard formula (Powell et al. 1984; Sacks & Roy 1982) (Equation 1):

$$PCSA = \left(\frac{Vmusc}{Lfasc}\right) cos\theta$$

When a tendon was present it was dissected down to its insertion onto the bone together with the muscle. The tendon was then transected at the musculotendinous junction when a clear separation became apparent and stretched on a flat surface. We then measured lengths with a standard ruler or flexible measuring tape (±1mm), and tendon mass was also measured using the same instrumentation as for the muscles.

Tendon cross-sectional area (TCSA) was calculated using tendon length (L_{ten}); from muscle origin to bony insertion; and tendon mass (M_{ten}) as follows (Equation 2):

$$TCSA = \frac{Mten}{1120Lten}$$

Where 1120 kg m^{-3} is assumed as the density of tendon (Hutchinson et al. 2014; Ker 1981).

Statistical analysis

Ontogenetic scaling relationships of (non-normalized) muscle properties were analysed using reduced major axis ("Model II") regression for $\log_{10}$ of each property vs $\log_{10}$ body mass using custom-designed R software code (R Development Core Team 2010) code. A Shapiro-Wilk test was performed to assess normality of distribution of the residuals, and the *p* value for significance was set to <0.05. The inclusion criteria for data presented were: Datasets first had to have a *p* value <0.05 in the above described Shapiro-Wilk test. If this *p* was >0.05, the data were then tested for the presence of outliers (which were set at ±2 standard deviations [SD] from the mean) and outliers removed. The RMA linear regression was performed again using this dataset and again, data were only presented if the *p* value for distribution of residuals was <0.05. Once the datasets were defined, R^2 correlation values and upper and lower bounds of the 95% confidence interval (CI) were calculated to assess the spread of data points around each regression line.

In order to obtain relative values to compare results from individuals of different size, muscle mass, PCSA and F_{length} were normalized to body mass (BM) by dividing each value by the subject's BM, $BM^{0.67}$ and $BM^{0.33}$ respectively. We used body mass (BM) as our independent variable and the target architectural parameter as our dependant variable. Overall, we followed a similar approach as that described by Allen et al. (2010,2014).

Briefly, for two objects to be considered geometrically similar (and thus for an isometric scaling pattern to be inferred), areas should scale to the square product of lengths and volumes to the cube of lengths. Because mass is a volumetric property, the dependant variable is considered to scale isometrically if the mass of the structure scales with BM^1, areal properties (PCSA, TCSA) scale to $BM^{0.67}$ and lengths scale to $BM^{0.33}$, whereas angles and other non-dimensional variables should scale as BM^0.

Results

We obtained 6524 measurements of seven different muscle-tendon architectural parameters from 34 pelvic limb muscles and four pelvic limb bones in 17 emus from 3.6 to 42 kg of body mass. We found strong evidence for positive allometric scaling for many of these architectural parameters, as described below. To aid interpretation of our results, we have divided the muscles of the limb into proximal (those acting mostly on the hip and knee joints) and distal (those acting on the ankle, foot and digits) groups and have used this division to compare trends between the two regions.

Bone lengths

The lengths of the four bones scaled with moderate positive allometry (expected slope representing isometry would be 0.33). The femur had the least marked allometric exponent (0.38), whilst the tarsometatarsus the greatest (0.44), the tibiotarsus had a slope value of 0.41 and for the 1st phalanx of the second digit (P1) the value was 0.39 (for full results see Table 2).

Myology, architectural characteristics of muscles and functional interpretation

We classified a total of 34 muscles in Table 1. As noted by Regnault et al. (2014), there is no patellar ossification in the knee joint of emus, unlike ostriches and some other palaeognaths as well as most extant birds. Although muscle origins, insertions and paths were generally found to agree with previous publications (Haughton 1867; Patak & Baldwin 1998; Vanden Berge & Zweers 1993) and hence detailed re-description is unnecessary, there were a few muscles for which we have found some differences worth noting, or for which we needed to use methodological simplifications:

M. iliotibialis lateralis pars postacetabularis (IL): The distal fusion and similar actions of both parts of the IL muscle (Fig.1) meant that, in order to avoid dissection errors when finding the division between the cranial and caudal parts of the muscle, we measured and presented them together.

M. iliotrochantericus cranialis (ITCR): Although this was a clear, separate muscle in most specimens (Fig. 2), it was found to be fused with the ITM in two specimens of body mass ~20 kg, which is a common finding in birds (Gangl et al. 2004)

M. ischiofemoralis (ISF): This small muscle is difficult to detect and dissect, which is likely to have affected the accuracy of the data obtained from it (leading to lower R^2 values and wider 95% CI ranges). Its action is likely to involve fine motor control, proprioception and stabilisation of the hip joint, given its very small size. Some studies have considered this muscle to be absent (or fused with other muscles; e.g., CFP) in emus (Haughton 1867; Patak & Baldwin 1998), which would be unusual for any birds. The origin and insertion of the muscle that we label the ISF (Fig. 3) is best interpreted as a reduced -- but still present – muscle, similar to that in ostriches (Gangl et al. 2004; Zinoviev 2006).

M. caudofemoralis pars pelvica (CFP): We consider, contrary to other reports (Haughton 1867; Patak & Baldwin 1998), that this muscle is present in emus (Fig. 2). Prior studies classified this muscle as the "iliofemoralis" but we agree with the *Nomina Anatomica Avium* (Vanden Berge & Zweers 1993) and other reports (Gangl et al. 2004; Hutchinson 2004a; Hutchinson et al. 2014; Zinoviev 2006) that it is present in ratites, related to a reduced portion of the large caudofemoralis muscle that is ancestrally present in tailed reptiles (Gatesy 1999). There is no evidence of a caudalis part to the M. caudofemoralis in emus, unlike in ostriches (Gangl et al. 2004) and some other ratites, so this sub-division of the CFP is either fused to the CFP or lost.

M. ambiens (AMB): We found this muscle to have two insertions, previously unnoticed: a tendinous one onto the tibia and a fleshy one onto the distal femur. Unusual modifications of this muscle seem common in ratite birds (Hutchinson et al. 2014)

M. popliteus: This is a short, deeply positioned, fleshy muscle with multiple fibrous planes within it, originating on the caudolateral, proximal aspect of the tibiotarsus and inserting onto the medial side of the proximal fibula (Fig. 3). It is likely a stabiliser or pronator/supinator of the fibula, as in ostriches (Fuss 1996), and may act as a proprioceptive or ligament-like structure.

Normalized data for individual muscles

To allow relative comparisons between muscle measurements, we normalized data from only the 16 month old (Group 3, adult birds) emus. Data are only presented for adult emus so as not to influence the relative proportions due to ontogenetic allometry. The entire ontogenetic data set was analysed similarly with negligible differences found, indicating that the relative patterns seen between muscles for adults are present in very young birds as well. Data for muscle mass, fascicle length and PCSA are presented in Figure 4. The largest relative muscles with regards to mass were three proximal (ILPO, ILFB and IC) and three distal muscles (GM, FL and GL). This order changes when muscles are ranked according to PCSA because parallel-fibred muscles tend to drop down the list, with the large ILPO being the only parallel-fibred muscle seen in the top 10 of a list that is otherwise dominated by distal muscles (FL, GM, GL and FPDIII). On the other hand, when fascicle length is compared, the three parts of the gastrocnemius (GIM, GM and GL) are the only distal muscles listed amongst the 10 muscles with the longest fascicles. . The four muscles with the longest fascicles are the FCLP, IC, ILFB and ILPO.

Limb muscle masses

Total mass values of the hindlimb musculature represented a mean of 13.4±3% of BM, with the proximal limb musculature (PLM) representing 61±2% of limb muscle mass and the distal limb

muscles (DLM) accounting for the remaining 39±2%. However, if only values for the six largest birds (adults) are analysed, limb muscle mass accounts for 15±1% of BM. The limb muscle mass is only 11±3% of body mass in the five birds that were 4-6 weeks old.

Scaling regression analysis

The slopes of the reduced major axis regression lines for muscle properties vs. body mass are shown in Tables 3 and 4, with R^2 and 95% CIs, as well as represented in Figures 5 (A and B) and 6. Ranges of the slope and amplitudes of the CIs referred to below are the upper and lower bounds of the 95% CIs for the regression slopes. Scaling exponents and CIs are presented in Table 3. Scaling exponents and lines representing isometry are plotted in Figure 5A and 5B (M_m, L_f and PCSA) and Figure 7 (M_{ten}, L_{ten} and TCSA). In summary, there was strong positive allometry of muscle mass and mild positive allometry or isometry of fascicle length, leading to a marked positive allometry of PCSA.

Scaling of limb muscle masses

We found limb muscle mass as well as the masses of proximal (PLM) and distal limb muscles (DLM) to be tightly correlated with body mass across all three groups. The regression slope of limb muscle mass vs. BM was 1.16 (1.05<CI<1.29, R^2=0.96), whilst PLM had a value of 1.14 (1.02<CI<1.27, R^2=0.96) and DLM exhibited a slope of 1.20 (1.09<CI<1.32, R^2=0.97).

Consistent with the trends for the hindlimb more broadly, the individual muscles also generally showed positive ontogenetic allometry. Out of 34 muscles, 26 had slopes for M_m vs. BM with their lower CI limit >1 (consistent with positive allometry), and only eight (ITCr, ITM, IFI, ISF, FCLA, FMTL, AMB and FPPDII) had a lower CI boundary for the regression slope lower than 1 (indicating potential negative allometry). Of the 26 muscles showing positive allometry of M_m, we found strong positive allometry (regression slopes with the lower boundary of the CI greater than 1.1) in 18/34.

Similarly, scaling patterns of the muscle masses for the USA group of emus (Figure 6), showed similar scaling patterns to the UK group, with only five muscles having a lower CI boundary <1 (POP, ILPO, FPDIV, OBTII and FPDII) and the remaining having their CIs entirely within positive allometry values.

Scaling of muscle fascicle length

In general, fascicle length (L_f) was only moderately well correlated with body mass due to substantial variation in the data (a combination of inevitable measurement errors, sampling bias and true biological variation, as usual for muscle fascicle measurements (e.g., Allen et al. [2010,2014]) The datasets for four muscles (ISF, PIFLM, FPDII and FPPDII) had a *p* value>0.05, so these are not presented (Table 3). Of the remaining 30 muscles, only 16/30 had R^2 values >0.5. Scaling of L_f vs. BM showed a trend towards positive allometry for 18/30 muscles (lower limit of the slope's CI >0.33), and for the remaining 12 muscles a slope of 0.33 was included in the CIs, so isometry could not be ruled out.

Scaling of muscle PCSA

The lower boundary of the CIs of the scaling slope was greater than 0.66 (i.e., exhibiting positive allometry) for 27 muscles and a value <0.66 (suggesting a potential negative allometry of muscle PCSA in emus) was obtained for eight muscles (ITM, ITC, IFI, FMTL, AMB, TC and FPPDII) (Table 3).

Scaling of tendon mass

We recorded tendon characteristics for 28 muscles (Table 4); the six muscles excluded did not have a discrete tendon at either of their attachments (CFP, FCLA, FCLP, IC, PIFLM, POP). We encountered difficulties in achieving a consistent method for tendon dissection and measurement of muscles with thin (IFE, AMB), very short (ISF and IFI) or multiple tendons (FMTM, FMTIM), which lead us to exclude data from these as well. The tendon of the GIM was included with the GM tendon, and the

FMTL tendon was not measured because the muscle was transected at the proximal aspect of the large patellar tendon for studies of patellar tendon morphology by Regnault et al. (2014). Thus data are presented for the tendons of 20 muscles. The major gastrocnemius tendon resulting from the fusion of the tendons of the three gastrocnemius muscles was dissected by transecting the tendon of the GL at the site of fusion onto the common tendon; therefore the GM remained with the extensive common portion of the tendon, which distally was transected at its insertion onto the fibrous scutum at the level of the ankle joint.

The scaling slopes for tendon mass indicate positive allometry in 10 out of 20 tendons (lower CI boundary >1) across emu ontogeny. The masses for the remaining ten tendons scaled with isometry (lower CI<1.0, upper CI>1.2)..

Scaling of tendon length

We measured L_{ten} for the same 20 muscles for which we obtained tendon masses (Table 4), from the end of the muscle belly to the insertion. Statistical analysis of one muscle (ITCr) led to exclusion of this muscle because the p value was >0.05. For the other 19 tendons, the general scaling trend was towards strong positive allometry, with 16 muscles having the lower limit of the CI >0.33. In three muscles (FCM, GM, FL), the lower CI for tendon length was <0.33, indicating isometry for length in these tendons. Given these patterns, we infer a general trend for positive allometry of tendon length in growing emus.

Scaling of tendon cross-sectional area

Average TCSA was calculated for the same 20 tendons as above (Table 4). The dataset for ILPO had a *p* value >0.05 and was excluded. Of the 19 remaining tendons, 10 showed a lower CI limit of the slope consistent with positive allometry (>0.66). The remaining nine tendons showed ontogenetic isometry for TCSA.

Discussion

Emus, like other ratites and other precocial birds, must have locomotor independence from hatching and develop into large, running adult birds within 16-18 months (Davies & Bamford 2002). Taking into consideration their initial development within the egg, their ontogeny poses interesting questions about their locomotor development, related to our study's aims, such as: How do muscle structure and anatomy change to accommodate precocial development in emus? What are the strategies that growing emus use to maintain tissue mechanical safety factors during rapid development of cursorial morphology and high-speed locomotor abilities? Our data suggest some answers to these questions, as follows.

Scaling patterns across ontogeny

We found positive allometry of emu pelvic limb muscle masses, indicating that most muscles get become significantly more powerful (in relative and absolute terms) as the animals grow. However, the functional relevance of this observation is slightly mitigated by a less marked positive allometry of PCSA (and therefore maximal muscle force), driven by a trend for fascicle length that is closer to isometry (i.e., preserving geometric similarity).

In the proximal part of the pelvic limb of emus, the developmental and functional mechanics appear to rely on the arrangement of large and metabolically expensive muscles (ILPO, ILFB, IC, FCLP and FMTL) to provide the wide range of motion of the knee joint (and hip, during faster running) in combination with a relatively short femur that scales close to isometry. This arrangement also leads to a proximal to distal gradient of muscle mass, which has been previously reported for other birds (Paxton et al. 2010; Smith et al. 2006) and has long been thought to favour energy-savings by

keeping the distal end of the limb light and its muscles dependent on springy tendons. The proximal-distal gradient also concentrates large, power-generating muscles in the proximal limb (Alexander 1974; Alexander 1991) with large moment arms (Hutchinson et al. 2014; Smith et al. 2007) and thus the ability to produce the considerable joint moments needed for high-speed running (Hutchinson 2004a,b).

The distal limb, on the other hand, is heavily dependent on the triad of M. gastrocnemius (GL, GIM and GM) along with M. fibularis longus (FL); both ankle extensors; as well as M. tibialis cranialis (TC) and M. extensor digitorum longus (EDL); both ankle flexors. Combined, these muscles constitute 80% of the muscle mass and 60% of the force-generating capacity (PCSA) of this portion of the limb. The unusual proportion of body mass taken up by the ankle extensors has been noted before (Hutchinson 2004a) and is likely an ancestral characteristic of birds (e.g., Paxton et al. 2010) but is taken to an extreme in large ratites (e.g., Smith et al. 2006).

Further distally, the long and slender tarsometatarsus bone lends itself well as a support for the long tendons of the digital flexor muscles which in turn provide essential springs used in support and propulsion of the limbs and body. The relatively small muscles and long tendons of the digital flexors make them likely to operate mainly as energy storage devices at faster speeds, as seen in other species like horses and smaller running birds (Biewener 1998; Daley & Biewener 2011). The positive allometry of many tendon properties in emus is in line with this increase in force-generating capacity seen during ontogeny. As in most other birds, the tendons running along the tarsometatarsus are almost exclusively on the cranial and caudal (dorsal/plantar) side. It would also be interesting to know the effect on bone strains from this “bow and arrow” anatomical arrangement between the tarsometatarsus and the dorsal/plantar tendons to see if it influences the predominantly torsional loads experienced by the two proximal pelvic limb bones (Main & Biewener 2007).

For these spring-like tendons, a trade-off between muscle force and tendon elasticity does not seem to occur in emus. This lack of a trade-off is indicated by the similar scaling patterns of the cross-sectional areas of the digital flexor muscles and tendons, both of which trend towards positive allometry across emu ontogeny. As seen in other species (Ker et al. 1988), the relative increases in the cross-sectional areas of tendons might maintain tendon safety factors (maximal stresses before failure vs. *in vivo* maximal stress) as emus increase in size. However, tendons might also change their biomechanical properties (Young’s modulus) with age, as seen in other species (Shadwick 1990; Thorpe et al. 2014), therefore influencing biomechanical interpretations of the data presented here. Without measuring tendon elastic modulus with age, it is difficult to interpret how tendon stiffness and safety factor might change with age in emus.

To complement data from a prior study showing the scaling patterns of the cross-sectional areas of the femur and tibiotarsus of emus to be close to isometry (Main & Biewener 2007), here we analysed the scaling patterns of the lengths of the three longest limb bones and the first phalanx of the third toe. Our data indicate positive allometry of the two longer bones, the tibiotarsus (lower CI limit=0.37) and tarsometatarsus (lower CI limit=0.39), but a less marked positively allometric scaling trend for the femur (lower limit of CI=0.34) and for the first phalanx of digit III (lower CI limit=0.33). These results differ from those reported for another ratite, the greater rhea (*Rhea americana*), in which only the tarsometarsus showed positive allometry (Picasso 2012a) but interestingly are in line with general interspecific scaling exponents found for pelvic limb bone lengths across different species of palaeognaths (Cubo & Casinos, 1996). Considering our results, if similar cross-sectional geometry is assumed along the length of the bone shafts, this would lead to an increase in strains (at least in bending, due to larger moments) at the mid-shaft with increasing body mass. However, changes in cross-sectional areal geometry have been shown to lead to slight positive allometry of the cross-sectional geometry of avian limb bones across species (Doube et al. 2012) and ontogenetically (Main & Biewener 2007). As these geometrical changes might not suffice to explain

the increases in strain magnitudes seen during ontogeny, they leave unexplained the role of internal forces (of soft tissues) on bone mechanics and consequently their influence on bone morphology during growth.

Although there are very limited data on the ontogeny of skeletal muscle physiology, experiments in mice and cats (Close 1964; Close & Hoh 1967) demonstrate that although muscle force: velocity parameters change from newborns to adults, these changes appear to occur in a relatively short period and therefore newborn muscle, after the first few days of life, becomes similar to that of adults. However, mice and cats, like many other mammals, are born with neuromotor immaturity (Muir 2000), in contrast to emus. It is therefore reasonable to speculate that, like other birds (Gaunt & Gans 1990), emus are unlikely to have appreciable changes in muscle physiology during growth. Thus changes in functional (e.g., maximal force-generating capacity) and biomechanical parameters should be detectable by anatomical studies such as ours.

Few studies have quantified the ontogenetic scaling patterns of limb musculature in birds (Carrier & Leon 1990; Dial & Carrier 2012; Paxton et al. 2014; 2012b; Picasso 2014), but positive allometry predominates in the muscle masses involved in the major adult mode of locomotion (flying vs. cursorial). In the Californian gull, the M. gastrocnemius scaled isometrically but the M. pectoralis had strong positive allometry with an inflection point when the fledglings started exercising their wings (Carrier & Leon 1990). Paxton et al. (2014; also 2010) recently reported the ontogenetic scaling patterns of the musculature of a highly modified galliform, the broiler chicken. These birds, unsurprisingly due to their selective breeding, were found to have positive allometry of muscle masses of the main pelvic limb muscles but isometry of the fascicle lengths (Paxton et al. 2014), a pattern that is nonetheless similar to our findings. Picasso et al. (2012b) found quite similar scaling patterns across rhea ontogeny: an average 64-fold increase in pelvic limb muscle mass from 1 month of age to adulthood whilst only a 34-fold increase in body mass. In a later study, where scaling exponents were calculated, a more generalised positively allometric scaling was found in these South American ratites compared to emus: with all muscle masses but two (where isometry was evident) scaling with positive allometry (slopes ~1.3). Total limb muscle mass of rheas scaled with an exponent of 1.18 (Picasso 2014), which is similar to our value of 1.16 .Together, these data suggest that positive allometry prevails across ontogeny for leg muscles in extant birds with precocial development; potentially a homologous feature of their development that is quite unlike the isometry prevailing in their closest extant relatives, Crocodylia (Allen et al., 2010,2014).

Dial and Carrier (2012) suggested that birds must optimise their energy consumption to achieve their ultimate functional gait whilst channelling resources to their precocial gait (Dial & Carrier 2012) (running vs. swimming or flying). Ratites are unusual for birds in that they solely have terrestrial gaits throughout their life and, in the case of emus, their wings have atrophied to such an extent that they should not present much metabolic competition to hindlimb development. Considering the approximately isometric overall scaling of kinematic parameters (e.g., stride lengths, stride frequencies, duty factors) seen in ratites (Main & Biewener 2007; Smith et al. 2010), it is likely that this increase in muscle masses will lead to a limb that is adapted for power production and perhaps (considering our less allometric tendon results) elastic energy storage/return. The former is also supported by metabolic studies which found a predominance of fast fibres in the M. gastrocnemius of adult emus (Patak 1993), although more studies of muscle physiology in emus and other ratites would be valuable.

The need for locomotor independence and high performance in vulnerable, young, precocial and cursorial birds might favour allometry of muscle architecture (Carrier 1996). If so, could adult muscle phenotypes be a reflection of the locomotor needs during early development and therefore be overdesigned for their demands? Alternatively, negative allometric scaling in the musculoskeletal system may occur as seen in goats (Main & Biewener 2004) and jackrabbits (Carrier 1983). It is hard

to draw an inference from our data, because the overall positive allometry seen in the pelvic limb musculature could indicate a necessity to grow faster and stronger to adulthood to compensate for a juvenile disadvantage or could reflect selective pressures on the locomotor ontogeny of emus in which muscles congenitally primed for fast growth during adolescence could lead to continued growth past an optimum in adulthood. Although direct measurements of maximal performance of complex locomotor systems is problematic, a modelling approach using the data presented here could be a valid approach to answer this question.

How well are farmed emus representative of the species overall?
Although emu farming is relatively common, its goal is to extract meat, oil and skin and therefore these birds are not bred in captivity for their locomotor behaviour, nor do they suffer strong predatory pressures on it. The diet of captive bred birds as well as their relative sedentary regime when compared to wild animals is likely to influence tissue development and distribution. However, as farming of these birds is a recent activity and it is not a highly specialised or intense process as with other domesticated species (Goonewardene et al. 2003), it is unlikely that heritable traits of the emu musculoskeletal system have been significantly altered. Therefore, we expect the muscle distribution and scaling patterns of our emus to be similar to wild emus.

By presenting muscle mass data from two distinct groups of birds (UK and USA groups), we established that these groups at least have similar scaling patterns, ruling out any potential bias imposed by different breeding regimes. With regards to diet, it was apparent that our birds were carrying a significant amount of subcutaneous and peritoneal fat; likely encouraged by their *ad libitum* access to a commercial pelleted diet. The influence of body fat on our scaling results is hard to test with the available data, but Hutchinson et al. (2014) noted a possible reduction in relative muscle masses in wild vs. captive bred ostriches, which could also apply to emus. Regardless, it is less certain that the scaling patterns for muscle/tendon architecture observed here would differ in wild vs. captive emus.

Conclusions
We have provided a new dataset on the ontogenetic scaling of pelvic limb anatomy and muscle architectural properties of a cursorial bird (the first complete architectural dataset of its kind), and we have done this using a group of 17 emus across a tenfold increase in body mass. A marked trend of positive allometry of muscle masses and PCSAs is accompanied by less marked positive allometry of fascicle lengths. Tendons, specially the long digital flexors, also demonstrate positive allometry of their lengths, as do the two longer limb bones (tibiotarsus and tarsometatarsus). We have illuminated the ontogenetic adaptation of the musculoskeletal system in an extreme example of size variation during rapid growth. Our dissections refined the myology of the pelvic limb in emus (Table 1 and Figures 1-3) and found some anatomical aspects that were previously misunderstood. This is important, as functional studies depending on inaccurate anatomical accounts of the myology could obtain unrealistic results from biomechanical models using such data (Goetz et al. 2008; Hutchinson et al. 2014). This work should be a valuable resource for future functional, comparative and evolutionary studies of emus, other birds and extinct related animals.

Acknowledgements

We thank Jack Machale, Emily Sparkes, Kyle Chadwick, Charlotte Cullingford, Sophie Regnault and Chris Basu who helped with the dissections. Craig McGowan provided assistance with muscle dissections in the USA emu sample. A special thank you goes to Vivian Allen for providing the custom designed R code that we used to perform the regression analysis, as well as valuable intellectual discussions. We also thank Ashley Heers and Diego Sustaita as well as an anonymous

506 reviewer and reviewer Trevor Worthy for their helpful comments on an earlier draft of this
507 manuscript.

PeerJ PrePrints

508 **Tables and table captions**

509 **Table 1.** Pelvic limb muscles of emus and their apparent actions.

Muscle	Abbreviation	Origin	Insertion	Action
M. iliotibialis cranialis	IC	Dorsal edge of preacetabular ilium	Insertion on the medial aspect of the proximal tibiotarsus	Main: Hip flexion; knee extension/flexion Other: Hip medial rotation, adduction
M. iliotibialis lateralis (cranial and caudal portions)	ILPO	Lateral edge of acetabular ala	Craniolateral proximal tibiotarsus (cranial and lateral cristae cnemiales) via aponeurosis (combined with FMTL)	Main: Hip extension,abduction; knee extension Other: Hip medial/lateral rotation
M. iliotrochantericus cranialis	ITCr	Cranial surface of preacetabular ilium	Lateral aspect of the femoral trochanteric crest (distal to IFE insertion)	Main: Hip flexion, medial rotation Other: Hip abduction/adduction
M. iliotrochantericus medialis	ITM	Craniodorsal surface of preacetabular ilium	Lateral aspect of the femoral trochanteric crest (proximal to IFE insertion)	Main: Hip flexion, medial rotation Other: Hip abduction/adduction
M. iliotrochantericus caudalis	ITC	Ala preacetabularis ilii: fossa iliaca dorsalis	Lateral aspect of the femoral trochanteric crest	Main: Hip flexion, medial rotation Other: Hip abduction/adduction
M. iliofibularis	ILFB	Ala postacetabularis ilii: facies lateralis	Proximal third of the corpus fibulae	Main: Knee flexion;, hip extension Other: Hip abduction
M. iliofemoralis externus	IFE	Crista iliaca dorsalis, dorsal to foramen acetabulum	Lateral side of femoral trochanteric crest (between ITC and ITM insertions)	Main: Hip flexion, abduction Other: Hip medial/lateral rotation
M. iliofemoralis internus	IFI	Ventral preacetabular ilium	Medial side of proximal femoral shaft; tubercle	Main: Hip flexion, adduction Other: Hip medial/lateral rotation
M. ischiofemoralis	ISF	Cranial margin of the foramen ilioischiadicum	Proximal caudal femur under origin of FMTL	Main: Hip abduction, lateral rotation Other: Hip flexion/extension
M. caudofemoralis p. pelvica	CFP	Caudolateral ilium and ischium	Proximal caudomedial femur	Main: Hip extension Other: Hip lateral rotation, abduction
M. flexor cruris lateralis pars pelvica	FCLP	Caudolateral corner of pelvis	Proximal craniomedial tibiotarsus	Main: Hip extension, abduction Other: Medial rotation of hip and knee; knee flexion
M. flexor cruris lateralis pars accessoria	FCLA	By a raphe from the distal third of the FCLP	Caudomedial femoral shaft	Main: Hip extension, abduction Other: Hip medial rotation
M. flexor cruris medialis	FCM	Caudolateral extremes of ischium and pubis	Via split cranial aponeurosis: on the caudal femoral shaft, and on the caudoproximal	Main: Hip extension, abduction; knee flexion Other: Hip medial rotation

PeerJ PrePrints

PeerJ PrePrints | http://dx.doi.org/10.7287/peerj.preprints.508v2 | CC-BY 4.0 Open Access | rec: 3 Dec 2014, publ: 3 Dec 2014

			tibiotarsus, caudodistally to the insertion of the FCLP.	
M. puboischiofemoralis p. lateralis and p. medialis	PIFLM	Along the length of the lateral ischium	Via thin tendinous insertion onto the caudal aspect of the femoral shaft	Main: Hip extension, abduction Other: Hip lateral rotation
M. femorotibialis lateralis (Cranial, intermediate and caudal portions)	FMTL	Caudolateral surface of femoral shaft. With 3 fused parts: cranial, intermediate and caudal	Crista cnemalis of tibiotarsus via a thick patellar tendon (no ossified patella) with ILPO	Knee extension
M. femorotibialis intermedialis	FMTIM	Cranial surface of the proximal femoral shaft	Medial side of crista cnemalis cranialis of tibiotarsus	Knee extension
M. femorotibialis medialis	FMTM	3 distinct heads originating from the medial surface of the femur, cranial and caudal portions on the proximal third and distal portion on the distal third	Proximo-medial extremity of tibiotarsus	Knee flexion, adduction
M. obturatorius medialis (Ilium – Ischium part)	OMII	Surface of fenestra ilioischium	Long tendon that passes through the foramen ilioischiadicum and inserts onto the lateral side of the femoral trochanteric crest	Main: Hip lateral rotation Other: Hip flexion, adduction
M. obturatorius medialis (Ischium – pubis part)	OMIP	Surface of fenestra ischiopubica	As OMII	Main: Hip lateral rotation Other: Hip flexion, adduction
M. ambiens	AMB	Cranial pubic rim (preacetabular process)	Two insertions on the medial knee ligaments, one tendinous and the other one fleshy	Main: Hip adduction; knee flexion Other: Hip medial rotation
M. gastrocnemius lateralis	GL	Lateral condyle of femur, aponeurosis of M. Iliotibialis and tendon from cranial fibula	Tendons fusing to form a thick fibrous calcaneal pad, onto caudal side of tarsometatarsus (Calcaneal scutum)	Main: Ankle extension; knee flexion
M. gastrocnemius medialis	GM	Aponeurosis of M. Iliotibialis and facies gastrocnemialis, connecting to the medial surface of the proximal tibia	As GL	Main: Ankle extension; knee flexion
M. gastrocnemius Intermedius	GIM	Craniolateral femur, adjacent of the origin of FHL muscle	As GL and GIM	Main: Ankle extension; knee flexion
M. fibularis longus	FL	Proximal origin from medial distal patellar ligament and craniolaterally onto proximal tibiotarsus.	Two tendinous insertions: Plantar calcaneal scutum and joining the tendon of FPDIII	Main: Ankle extension Other: Knee flexion; toe flexion via FPDIII tendon
M. tibialis cranialis c. tibiale and c. femorale	TC	2 heads: A fleshy one onto the proximal cranial tibiotarsus, and via a thick tendon onto the cranial aspect of the lateral trochlear ridge of the femur	Cranial side of proximal tarsometatarsus	Main: Ankle flexion Other: Knee extension (femoral head)
M. popliteus	POP	Medial side of proximal fibula	Caudal side of proximal tibiotarsus	Main: Fibular rotation
M. flexor perforatus digiti II	FPDII	Via origin of FPDIII	Splits into 2 branches at level of proximal phalanx to insert on either side of middle	Main: Digit II flexion Other: Ankle extension

PeerJ PrePrints

PeerJ PrePrints | http://dx.doi.org/10.7287/peerj.preprints.508v2 | CC-BY 4.0 Open Access | rec: 3 Dec 2014, publ: 3 Dec 2014

			phalanx, ventrally	
M. flexor perforatus digiti III	FPDIII	2 tendons: Cranial fibula and medial side of the medial condyle of the femur	Proximal phalanx, small portion fused to FPPDII tendon in some specimens, ventrally	Main: Digit III flexion Other: Ankle extension
M. flexor perforans et perforatuss digiti II	FPPDII	Deep fibular tendon of GL muscle	Middle phalanx of digit II, ventrally	Main: Digit II flexion Other: Ankle extension
M. flexor perforans et perforatus digiti III	FPPDIII	Lateral knee ligaments and FPDIV origin	Middle phalanx of digit III, ventrally	Main: Digit III flexion Other: Ankle extension
M. flexor perforatus digiti IV	FPDIV	Superficial side of FPDIII origin	Proximal and middle phalanges of digit IV, ventrally	Main: Digit IV flexion Other: Ankle extension
M. flexor hallucis longus	FHL	2 heads: lateral and caudal aspects of distal femur near condyles	Fuses with FDL tendon	Main: Ankle extension; knee flexion
M. flexor digitorum longus	FDL	2 heads: proximal tibiotarsus and distal third of fibula (3/4 of length)	Splits into 3 parts above MTP joint to insert onto the distal, ventral phalanx of each toe	Main: Digits II, III and IV flexion Other: Ankle extension
M. extensor digitorum longus	EDL	Cranial proximal tibiotarsus	Dorsal surface of each phalanx	Main: Digits II, III and IV extension; ankle flexion

510

PeerJ PrePrints

PeerJ PrePrints | http://dx.doi.org/10.7287/peerj.preprints.508v2 | CC-BY 4.0 Open Access | rec: 3 Dec 2014, publ: 3 Dec 2014

Bone	Scaling exponent	Lower 95% CI	Upper 95% CI	R^2
Femur	0.38	0.34	0.42	0.96
Tibiotarsus	0.41	0.38	0.45	0.97
Tarsometatarsus	0.44	0.39	0.49	0.96
First Phalanx (Dig III)	0.39	0.33	0.46	0.91

511 **Table 2.** Regression analysis results for the lengths of the four limb bones. The lower 95% boundary
512 (>0.33) demonstrates positive allometry of the tibiotarsus and the tarsometatarsus but results are
513 closer to isometry for the femur and first phalanx of digit III.

514

PeerJ PrePrints

	M_m vs BM					L_f vs BM					PCSA vs BM				
Muscle	*Outliers*	*Slope*	*Lower 95% CI*	*Upper 95% CI*	R^2	*Outliers*	*Slope*	*Lower 95% CI*	*Upper 95% CI*	R^2	*Outliers*	*Slope*	*Lower 95% CI*	*Upper 95% CI*	R^2
AMB	0	1.08	0.96	1.21	0.96	0	0.42	0.31	0.57	0.67	0	0.81	0.64	1.03	0.81
CFP	0	1.18	1.09	1.28	0.98	0	0.48	0.31	0.73	0.36	0	0.94	0.78	1.13	0.89
EDL	0	1.25	1.10	1.41	0.95	0	0.54	0.39	0.75	0.64	0	0.82	0.67	1.01	0.86
FCLA	1	1.16	0.95	1.43	0.87	1	0.36	0.24	0.53	0.51	1	0.89	0.73	1.09	0.87
FCLP	0	1.26	1.16	1.36	0.98	0	0.33	0.24	0.44	0.69	0	0.99	0.89	1.09	0.97
FCM	1	1.31	1.16	1.48	0.95	1	0.60	0.39	0.91	0.42	1	0.95	0.75	1.20	0.83
FDL	1	1.29	1.15	1.44	0.96	1	0.58	0.37	0.90	0.36	1	0.93	0.76	1.15	0.86
FHL	1	1.22	1.04	1.42	0.93	1	0.66	0.42	1.04	0.34	1	0.98	0.70	1.37	0.64
FL	0	1.32	1.23	1.42	0.98	0	0.44	0.33	0.58	0.73	0	0.98	0.84	1.16	0.91
FMTIM	0	1.24	1.05	1.48	0.90	0	0.64	0.43	0.97	0.40	0	0.99	0.70	1.41	0.57
FMTL	0	1.19	0.95	1.49	0.83	0	0.43	0.31	0.60	0.64	0	0.86	0.65	1.14	0.73
FMTM	0	1.29	1.05	1.59	0.86	0	0.45	0.29	0.70	0.31	0	0.99	0.80	1.22	0.85
FPDII	0	1.45	1.26	1.67	0.93		-	-	-	-	0	1.40	1.06	1.84	0.74
FPDIII	0	1.34	1.19	1.51	0.95	0	0.60	0.41	0.88	0.47	0	1.03	0.78	1.36	0.74
FPDIV	0	1.20	1.09	1.32	0.97	0	0.43	0.28	0.65	0.38	0	0.99	0.80	1.22	0.85
FPPDII	0	0.75	0.59	0.95	0.81	0	0.74	0.49	1.14	0.37	0	0.68	0.44	1.07	0.29
FPPDIII	0	1.29	1.15	1.45	0.96		-	-	-	-	0	0.98	0.72	1.34	0.67
GIM	0	1.32	1.01	1.73	0.75	0	0.46	0.34	0.63	0.69	0	1.03	0.72	1.48	0.54
GL	0	1.30	1.19	1.43	0.97	0	0.51	0.40	0.67	0.77	0	0.88	0.76	1.01	0.93
GM	0	1.24	1.14	1.33	0.98	0	0.34	0.26	0.43	0.77	0	0.93	0.82	1.06	0.95
IC	0	1.27	1.15	1.40	0.97	0	0.31	0.24	0.39	0.81	0	1.00	0.88	1.13	0.95
IFE	0	1.26	1.11	1.42	0.95	0	0.56	0.42	0.75	0.72	0	0.79	0.66	0.93	0.91
IFI	2	1.22	0.97	1.54	0.85	2	0.49	0.33	0.72	0.57	2	0.92	0.66	1.28	0.68
IB	0	1.32	1.22	1.42	0.98	0	0.36	0.30	0.44	0.89	0	0.98	0.89	1.07	0.97
ILPO	0	1.29	1.16	1.43	0.96	0	0.31	0.21	0.46	0.50	0	1.08	0.92	1.26	0.92
ISF	3	1.10	0.93	1.32	0.92	-	-	-	-	--	3	1.06	0.73	1.54	0.63
ITC	2	1.26	1.14	1.39	0.97	2	0.76	0.61	0.95	0.86	2	0.64	0.50	0.81	0.84
ITCr	0	1.16	0.99	1.36	0.92	0	0.37	0.27	0.50	0.68	0	0.89	0.70	1.13	0.80
ITM	2	1.12	0.83	1.51	0.75	2	0.78	0.49	1.23	0.39	2	0.89	0.55	1.45	0.29
OMII	0	1.23	1.10	1.39	0.95	0	0.73	0.46	1.15	0.27	0	1.05	0.76	1.45	0.65
OMIP	0	1.23	1.11	1.36	0.97	0	0.53	0.36	0.77	0.49	0	0.94	0.77	1.15	0.87
PIFLM	0	1.24	1.13	1.36	0.97	-	-	-	-	-	0	1.11	0.89	1.39	0.83
POP	2	1.44	1.17	1.76	0.88	2	0.68	0.41	1.13	0.22	2	1.15	0.88	1.51	0.79
TC	0	1.20	1.08	1.33	0.97	0	0.68	0.50	0.93	0.67	0	0.77	0.55	1.07	0.63

Table 3. Results of RMA linear regression of muscle architecture vs. body mass (BM) for the pelvic limb of *Dromaius novaehollandiae*, across ontogeny. M_m, muscle mass (kg); L_f, fascicle length (m), *PCSA*, physiological cross-sectional area (m^2).

PeerJ PrePrints | http://dx.doi.org/10.7287/peerj.preprints.508v2 | CC-BY 4.0 Open Access | rec: 3 Dec 2014, publ: 3 Dec 2014

	M_{ten} vs BM					L_{ten} vs BM					TCSA vs BM				
Tendon	*Outliers*	*Slope*	*Lower 95% CI*	*Upper 95% CI*	R^2	*Outliers*	*Slope*	*Lower 95% CI*	*Upper 95% CI*	R^2	*Outliers*	*Slope*	*Lower 95% CI*	*Upper 95% CI*	R^2
EDL	0	1.26	1.10	1.44	0.94	1	-0.81	-1.07	-0.61	0.75	0	0.86	0.61	1.22	0.58
FCM	0	1.31	1.01	1.69	0.86	0	0.46	0.27	0.79	0.34	0	1.05	0.78	1.43	0.81
FDL	1	1.22	1.08	1.39	0.95	1	0.43	0.36	0.51	0.91	1	0.81	0.70	0.93	0.94
FHL	1	1.29	1.09	1.53	0.91	1	0.45	0.34	0.60	0.74	1	0.87	0.75	1.01	0.93
FL	0	1.33	1.15	1.52	0.94	0	0.39	0.31	0.50	0.81	0	0.99	0.82	1.20	0.88
FPDII	0	1.26	1.03	1.53	0.87	0	0.63	0.40	0.97	0.32	0	1.09	0.76	1.57	0.56
FPDIII	0	1.38	1.21	1.58	0.94	0	0.43	0.36	0.52	0.88	0	1.01	0.82	1.24	0.86
FPDIV	0	1.17	1.05	1.31	0.96	0	0.42	0.37	0.48	0.95	0	0.76	0.67	0.86	0.95
FPPDII	0	1.34	0.95	1.88	0.60	0	0.78	0.58	1.06	0.69	0	0.80	0.50	1.27	0.24
FPPDIII	0	1.24	1.06	1.44	0.92	0	0.43	0.38	0.49	0.95	0	0.83	0.68	1.03	0.85
GL	0	1.63	1.19	2.23	0.66	0	0.89	0.59	1.36	0.38	0	0.95	0.69	1.30	0.66
GM	0	0.98	0.78	1.23	0.83	0	0.28	0.18	0.43	0.37	0	0.79	0.64	0.97	0.85
IB	1	1.03	0.79	1.33	0.79	1	0.51	0.35	0.73	0.57	1	0.81	0.53	1.23	0.43
ILPO	2	1.38	0.99	1.93	0.68	2	1.04	0.69	1.56	0.51	-	-	-	-	-
ITC	3	1.04	0.81	1.33	0.84	3	0.61	0.44	0.83	0.74	3	0.75	0.46	1.22	0.34
ITCr	1	1.02	0.76	1.36	0.73	-	-	-	-	-	1	1.18	0.80	1.74	0.52
ITM	7	1.37	0.76	2.46	0.43	6	0.72	0.37	1.42	0.09	7	1.19	0.61	2.33	0.21
OMII	0	1.26	0.98	1.62	0.79	0	0.71	0.53	0.94	0.72	0	0.75	0.51	1.10	0.48
OMIP	0	0.99	0.74	1.33	0.70	1	0.48	0.36	0.65	0.71	1	0.67	0.44	1.02	0.43
TC	0	1.06	0.85	1.30	0.85	0	0.50	0.34	0.73	0.47	0	0.75	0.56	1.00	0.71

Table 4. Results of RMA linear regression of tendon dimensions vs. body mass (BM) for the pelvic limb of *Dromaius novaehollandiae*, across ontogeny. M_{ten}, tendon mass (kg); L_{ten}, tendon length (m); *TCSA*, tendon cross-sectional area (m^2).

PeerJ PrePrints

PeerJ PrePrints | http://dx.doi.org/10.7287/peerj.preprints.508v2 | CC-BY 4.0 Open Access | rec: 3 Dec 2014, publ: 3 Dec 2014

521 **Figures and Figure Captions**

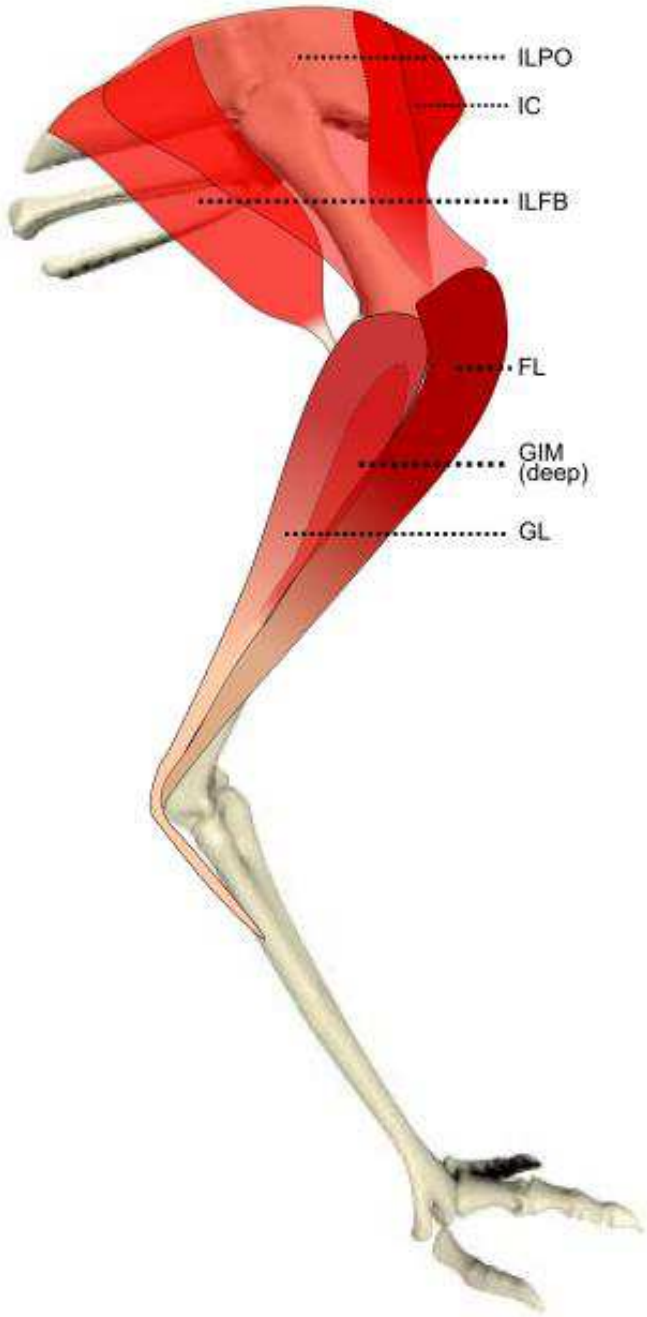

522

523 **Figure 1** Schematic anatomical representation of the most superficial layer of muscles, in lateral
524 view, of the pelvic limb of an adult emu.

525

526

PeerJ PrePrints

527

528

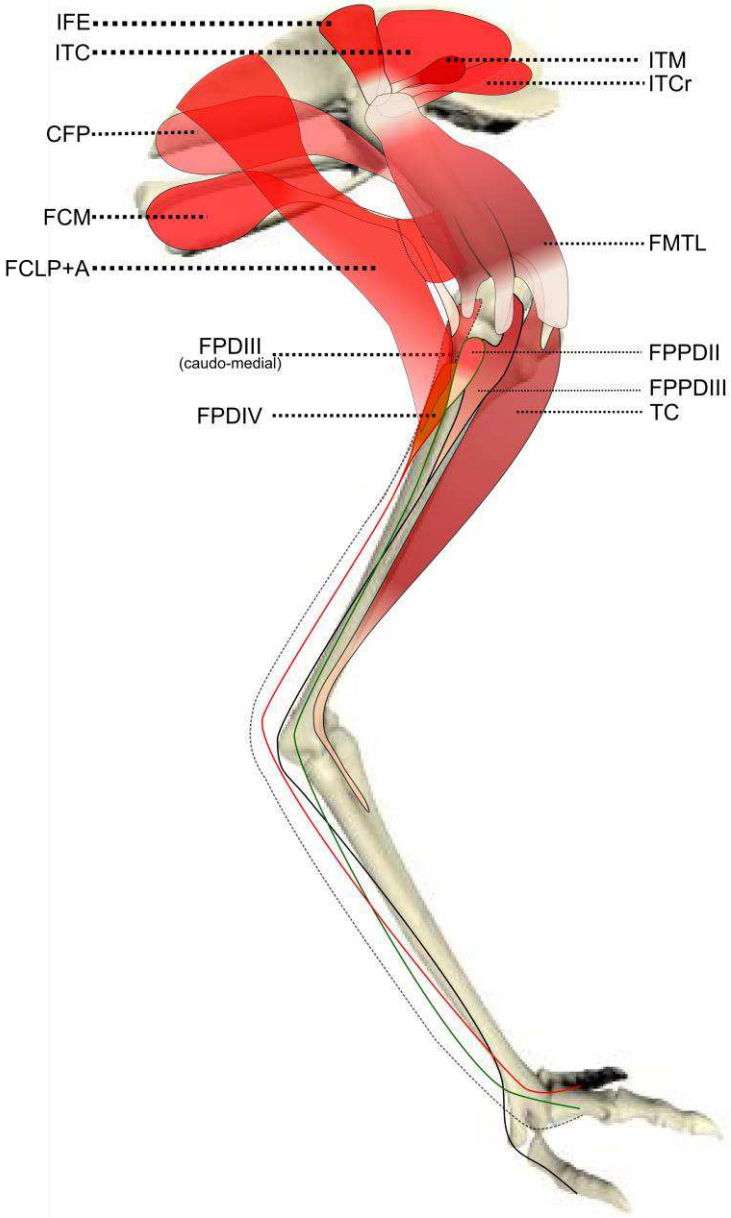

529

530 **Figure 2.** Schematic anatomical representation of the intermediate layer of muscles, from a lateral
531 view, of the pelvic limb of an adult emu.

PeerJ PrePrints

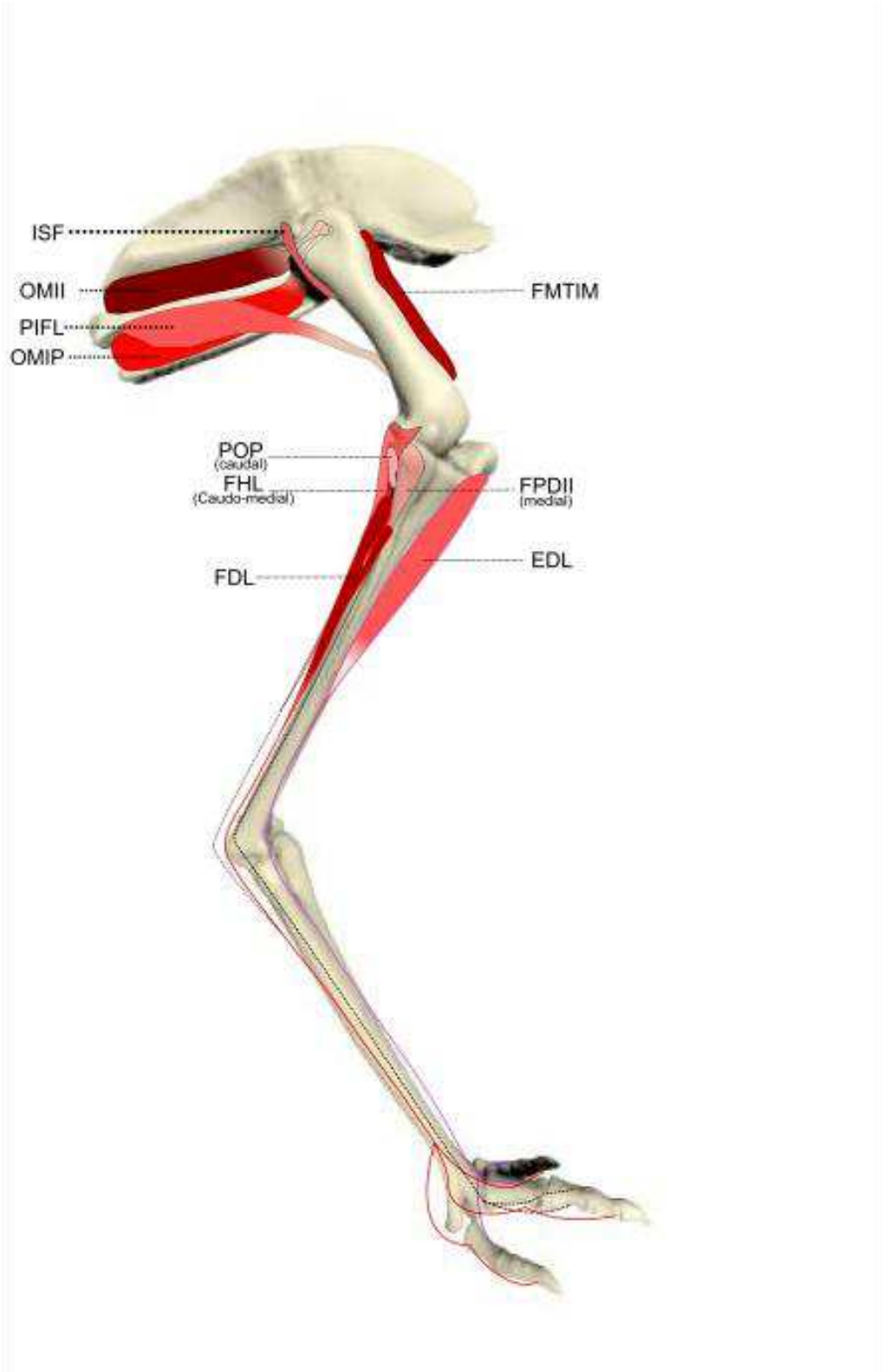

532

533 **Figure 3.** Schematic anatomical representation of the deeper layer of muscles, from a lateral view, of
534 the pelvic limb of an adult emu.

PeerJ PrePrints

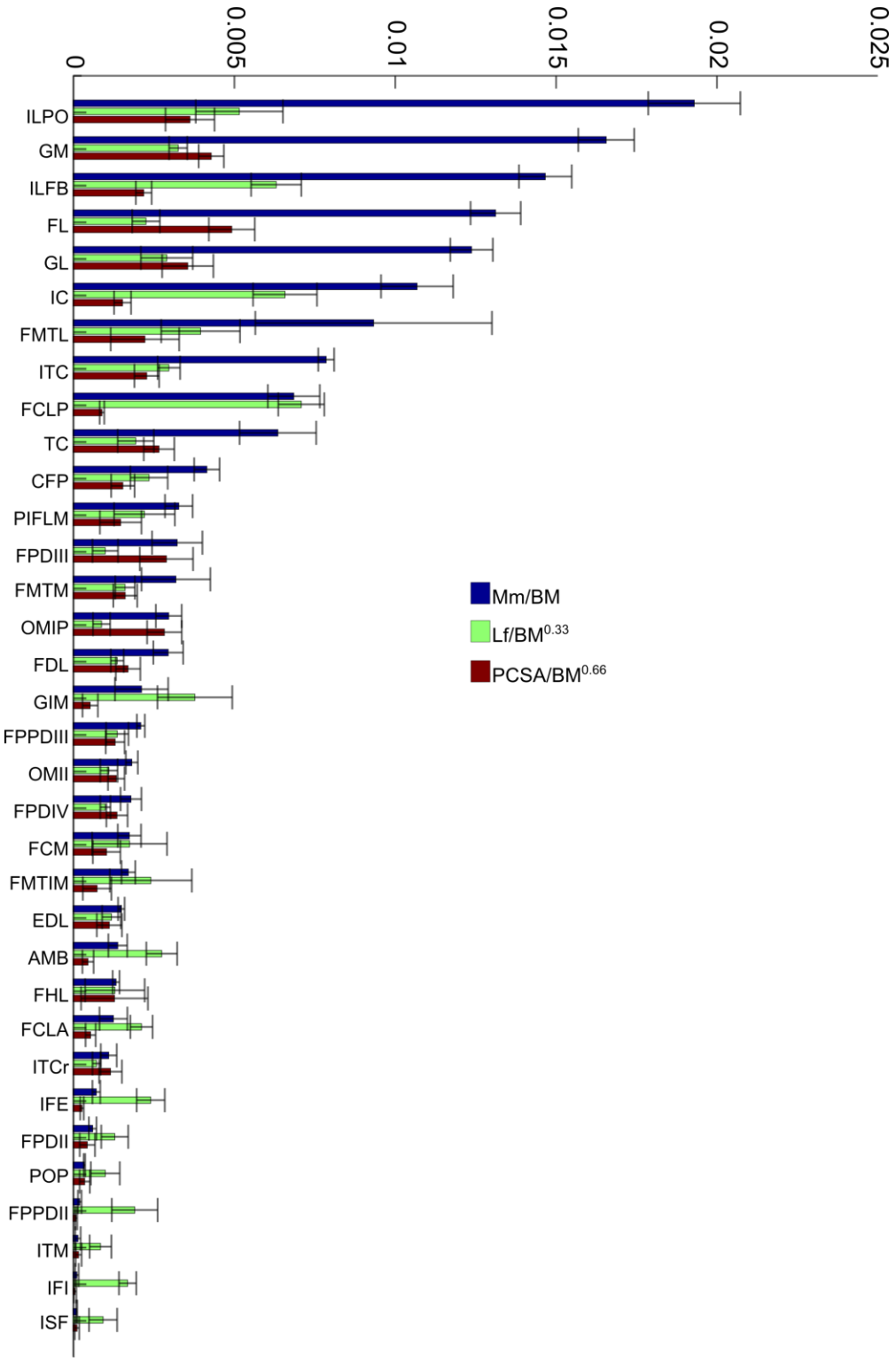

535

536 **Figure 4**. Normalized relative muscle parameters for individual muscles in emu pelvic limbs of the 16
537 month old birds only (Group 3; mean body mass 38.5 kg); mean values (error bars showing ±1 S.D.)
538 are shown. Abbreviations for muscles are in Table 1. The key on the right side of the figure shows
539 how muscle mass (M_m), physiological cross-sectional area (PCSA), and fascicle length (L_f) were
540 normalized. L_f values were adjusted to be 1/10 of the actual results in order to be of similar
541 magnitude to the others. Muscles are organised from top to bottom in decreasing order of muscle
542 mass.

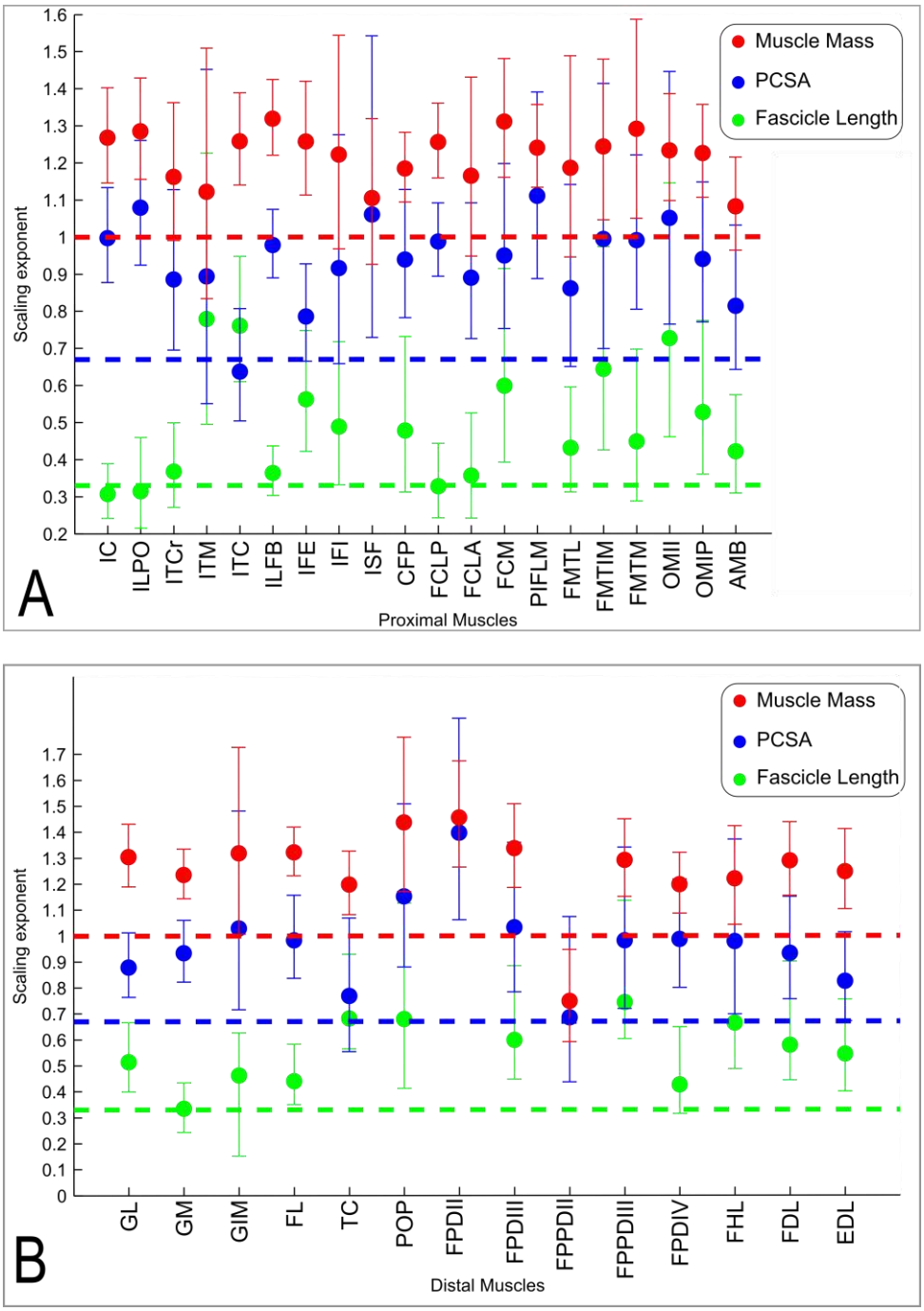

Figure 5. Ontogenetic scaling exponents and 95% confidence intervals (shown as error bars around mean exponent) for muscle mass (red), PCSA (blue) and fascicle length (green) for individual muscles in emu pelvic limbs. Abbreviations for muscles are in Table 1. Dashed lines indicate the expected isometric scaling exponent for each parameter. Data are for **A)** proximal limb muscles and **B)** distal limb muscles.

PeerJ PrePrints

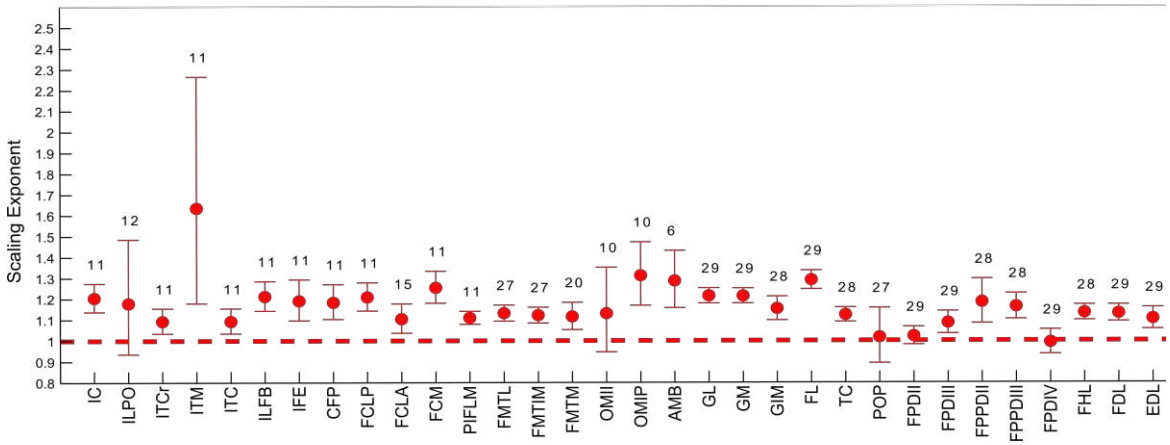

552
553 **Figure 6.** Ontogenetic scaling exponents and 95% confidence intervals for masses of individual
554 muscles in emu pelvic limbs, from the USA group. Abbreviations for muscles are in Table 1. Dashed
555 line indicates the expected isometric scaling exponent (1.0), and the number above each parameter
556 indicates the number of muscles included in each regression analysis.

557

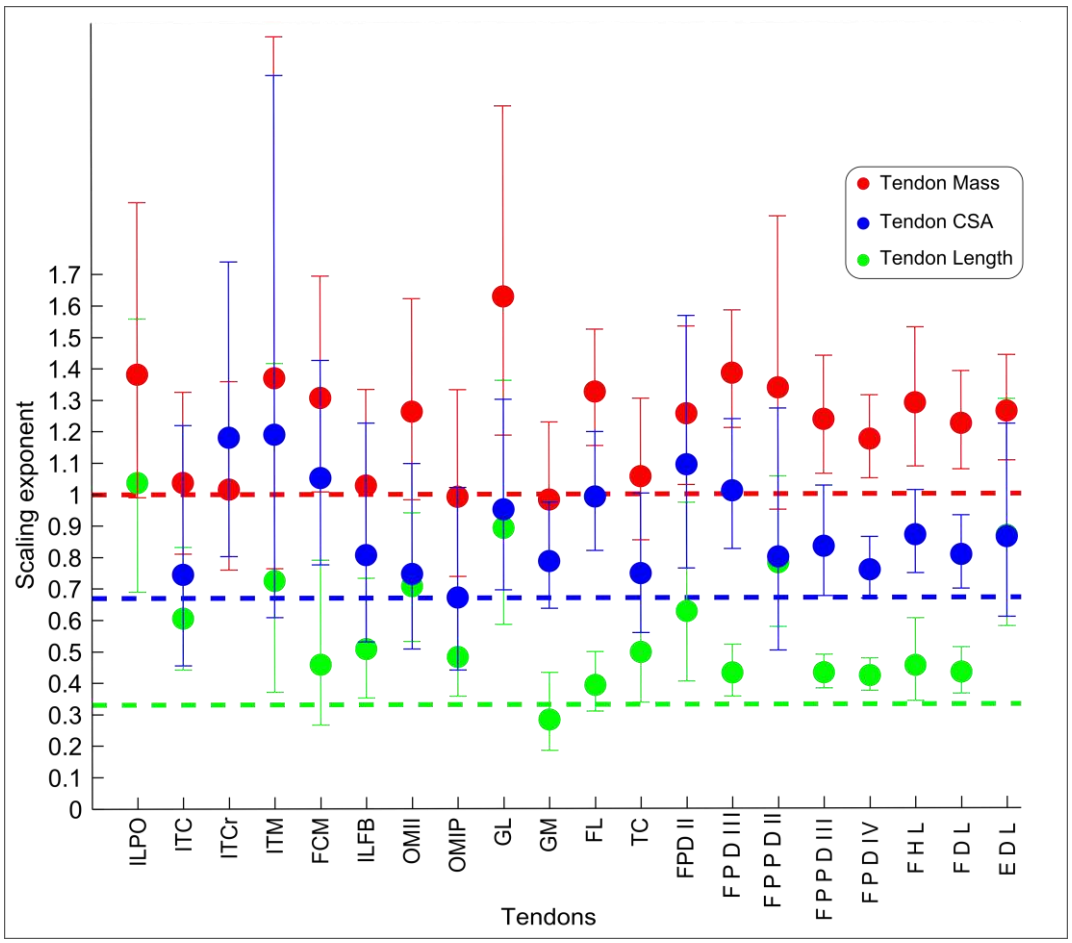

558

559 **Figure 7.** Ontogenetic scaling exponents and 95% confidence intervals for tendon mass (red),
560 average cross-sectional area (blue) and length (green) for 20 individual muscles in emu pelvic limbs.
561 Abbreviations for muscles are in Table 1. Dashed lines indicate the expected isometric scaling
562 exponent for each parameter.

563 **References**

564 Abourachid A. 2000. Bipedal locomotion in ratites (Paleognatiform): examples of cursorial birds.
565 *Ibis*:538-549.Alexander R. 1974. Mechanics of jumping by a dog *Canis familiaris*. *Journal of Zoology*
566 173:549-573.

567 Alexander R. 1991. Energy saving mechanisms in walking and running. *Journal of Experimental*
568 *Biology* 160:55-69.
569 Alexander R, Jayes A, Maloiy GM, and Wathuda E. 1979. Allometry of the limb bones of mammals
570 from shrews (*Sorex*) to elephant (*Loxodonta*). *Journal of Zoology* 189:305-314.
571 Allen V, Elsey RM, Jones N, Wright J, and Hutchinson JR. 2010. Functional specialization and
572 ontogenetic scaling of limb anatomy in *Alligator mississippiensis. Journal of Anatomy*
573 216:423-445.
574 Allen, V., Molnar, J., Parker, W., Pollard, A., Nolan, G. and Hutchinson, J. R. (2014), Comparative
575 architectural properties of limb muscles in Crocodylidae and Alligatoridae and their
576 relevance to divergent use of asymmetrical gaits in extant Crocodylia. *Journal of Anatomy*
577 225:569-582.
578 Bertram JE, and Biewener A. 1990. Differential scaling of the long bones in the terrestrial Carnivora
579 and other mammals. *Journal of Morphology* 204:157-169.
580 Biewener A. 1998. Muscle-tendon stresses and elastic energy storage during locomotion in the
581 horse. *Comparative Biochemistry and Physiology B* 120:73-87.
582 Biewener A.. 1982. Bone strength in small mammals and bipedal birds: do safety factors change with
583 body size? *Journal of Experimental Biology* 98:289-301.
584 Brown NT, Pandy MG, Kawcak CE, and McIlwraith CW. 2003. Force- and moment-generating
585 capacities of muscles in the distal forelimb of the horse. *Journal of Anatomy* 203:101-113.
586 Carrier D, and Leon L. 1990. Skeletal growth and function in the California gull (*Larus californicus*).
587 *Journal of Zoology* 222:375-389.
588 Carrier DR. 1996. Ontogenetic limits on locomotor performance. *Physiological Zoology* 69:467-488.
589 Carrier R. 1983. Postnatal ontogeny of the musculo-skeletal system in the black-tailed jackrabbit
590 (*Lepus californicus*). *Journal of Zoology* 201:27-55.
591 Close B. 1964. Dynamic properties of fast and slow skeletal muscles of the rat during development.
592 *Journal of Physiology* 173:74-95.
593 Close B, and Hoh J. 1967. Force:velocity properties of kitten muscles. *Journal of Physiology* 192:815-
594 822.
595 Cubo J, and Casinos A. 1996. Flightlessness and long bone allometry in Palaeognathiformes and
596 Sphenisciformes. *Netherlands Journal of Zoology* 47:209-226.
597 Daley MA, and Biewener AA. 2011. Leg muscles that mediate stability: mechanics and control of two
598 distal extensor muscles during obstacle negotiation in the guinea fowl. *Philosophical*
599 *Transactions of the Royal Society of London B: Biological Sciences* 366:1580-1591.
600 Davies SF, and Bamford M. 2002. *Ratites and Tinamous: Tinamidae, Rheidae, Dromaiidae,*
601 *Casuariidae, Apterygidae, Struthionidae*: Oxford University Press.
602 Dial KP, and Jackson BE. 2011. When hatchlings outperform adults: locomotor development in
603 Australian brush turkeys (*Alectura lathami,* Galliformes). *Proceedings of the Royal Society B:*
604 *Biological Sciences* 278:1610-1616.
605 Dial TR, and Carrier DR. 2012. Precocial hindlimbs and altricial forelimbs: partitioning ontogenetic
606 strategies in mallards (*Anas platyrhynchos*). *Journal of Experimental Biology* 215:3703-3710.
607 Doube M, Yen SC, Klosowski MM, Farke AA, Hutchinson JR, and Shefelbine SJ. 2012. Whole-bone
608 scaling of the avian pelvic limb. *Journal of Anatomy* 221:21-29.
609 Fuss FK. 1996. Tibiofibular junction of the South African ostrich (*Struthio camelus australis*). *Journal*
610 *of Morphology* 227:213-226.

611 Gangl D, Weissengruber GE, Egerbacher M, and Forstenpointner G. 2004. Anatomical description of
612 the muscles of the pelvic limb in the ostrich (*Struthio camelus*). *Anatomia Histologia*
613 *Embryologia* 33:100-114.
614 Gatesy SM. 1999. Guineafowl hind limb function. II: Electromyographic analysis and motor pattern
615 evolution. *Journal of Morphology* 240:127-142.
616 Gatesy SM, and Biewener AA. 1991. Bipedal locomotion: Effects of speed , size and limb posture in
617 birds and humans. *Journal of Zoology* 224:127-147.
618 Gaunt A, and Gans C. 1990. Architecture of chicken muscles: short-fibre patterns and their ontogeny.
619 *Proceedings of the Royal Society of London B: Biological Sciences* 240:351-362.
620 Gillooly JF, Brown JH, West GB, Savage VM, and Charnov EL. 2001. Effects of size and temperature
621 on metabolic rate. *Science* 293:2248-2251.
622 Goetz JE, Derrick TR, Pedersen DR, Robinson Da, Conzemius MG, Baer TE, and Brown TD. 2008. Hip
623 joint contact force in the emu (*Dromaius novaehollandiae*) during normal level walking.
624 *Journal of Biomechanics* 41:770-778.
625 Goonewardene LA, Wang Z, Okine E, Zuidhof MJ, Dunk E, and Onderka D. 2003. Comparative growth
626 characteristics of emus (*Dromaius novaehollandiae*). *Journal of Applied Poultry Research*
627 12:27-31.
628 Haughton S. 1867. The muscular anatomy of the emu (*Dromaius novaehollandiae*). *Proceedings of*
629 *the Royal Irish Academy* 9:487-497.
630 Hemmingsen AM. 1960. Energy metabolism as related to body size and respiratory surfaces, and its
631 evolution. *Steno Memorial Hospital and Nordinsk Insulin Laboratorium* 9:6:110.
632 Hokkanen JE. 1986. The size of the largest land animal. *Journal of Theoretical Biology* 118:491-499.
633 Hutchinson JR. 2004a. Biomechanical modeling and sensitivity analysis of bipedal running ability. I.
634 Extant taxa. *Journal of Morphology* 262:421-440.
635 Hutchinson JR. 2004b. Biomechanical modeling and sensitivity analysis of bipedal running ability. II.
636 Extinct taxa. *Journal of Morphology* 262:441-461.
637 Hutchinson JR, Rankin J, Rubenson J, Rosenbluth K, Siston R, and Delp S. 2014. Musculoskeletal
638 modeling of an ostrich (*Struthio camelus*) pelvic limb: Influence of limb orientation on
639 muscular capacity during locomotion. *PeerJ PeerJ PrePrints 2:e513v1*
640 *http://dx.doi.org/10.7287/peerj.preprints.513v1 (in review)*.
641 Ker R. 1981. Dynamic tensile properties of the plantaris tendon of sheep (*Ovis aries*). *Journal of*
642 *Experimental Biology* 93:283-302.
643 Ker RF, Alexander R, and Bennet M. 1988. Why are mammalian tendons so thick? *Journal of Zoology*
644 216:309-324.
645 Kleiber M. 1932. Body size and metabolism. *Hilgardia* 6:311-353.
646 LaBarbera M. 1989. Analyzing body size as a factor in ecology and evolution. *Annual Review of*
647 *Ecology and Systematics* 20:97-117.
648 Main RP, and Biewener AA. 2004. Ontogenetic patterns of limb loading, in vivo bone strains and
649 growth in the goat radius. *Journal of Experimental Biology* 207:2577-2588.
650 Main RP, and Biewener AA. 2007. Skeletal strain patterns and growth in the emu hindlimb during
651 ontogeny. *Journal of Experimental Biology* 210:2676-2690.
652 Maloiy GM, Alexander RM, Njau R, and Jayes AS. 1979. Allometry of the legs of running birds. *Journal*
653 *of Zoology* 187:161-167.
654 McMahon T. 1975. Allometry and biomechanics: limb bones in adult ungulates. *American Naturalist*
655 109:547-563.
656 Mendez J, and Keys A. 1960. Density and composition of mammalian muscle. *Metabolism-Clinical*
657 *and Experimental* 9:184-188.
658 Miller CE, Basu C, Fritsch G, Hildebrandt T, and Hutchinson JR. 2008. Ontogenetic scaling of foot
659 musculoskeletal anatomy in elephants. *Journal of the Royal Society, Interface* 5:465-475.
660 Minnaar P, and Minnaar M. 1998. *The Emu Farmer's Handbook*: Induna Company.

661 Muir GD. 2000. Early ontogeny of locomotor behaviour: a comparison between altricial and
662 precocial animals. *Brain Research Bulletin* 53:719-726.
663 Patak A. 1993. Structural and metabolic characterization of the muscles used to power running in
664 the emu (*Dromaius novaehollandiae*), a giant flightless bird. *Journal of Experimental Biology*
665 249:233-249.
666 Patak A, and Baldwin J. 1998. Pelvic limb musculature in the emu *Dromaius novaehollandiae* (Aves:
667 Struthioniformes: Dromaiidae): adaptations to high-speed running. *Journal of Morphology*
668 238:23-37.
669 Paxton H, Anthony NB, Corr SA, and Hutchinson JR. 2010. The effects of selective breeding on the
670 architectural properties of the pelvic limb in broiler chickens: a comparative study across
671 modern and ancestral populations. *Journal of Anatomy* 217:153-166.
672 Paxton H, Tickle P, Rankin J, Codd J, and Hutchinson J. 2014. Anatomical and biomechanical traits of
673 broiler chickens across ontogeny. Part II. Body segment inertial properties and muscle
674 architecture of the pelvic limb. *PeerJ 2:e473*.
675 Picasso MBJ. 2012a. Postnatal ontogeny of the locomotor skeleton of a cursorial bird: greater rhea.
676 *Journal of Zoology* 286:303-311.
677 Picasso MBJ, Tambussi CP, Mosto MC, and Degrange FJ. 2012b. Crescimiento de la masa muscular
678 del miembro posterior del Ñandu Grande (*Rhea americana*) durante la vida postnatal.
679 *Revista Brasileira de Ornintologia* 20:1-7.
680 Picasso MBJ. 2014. Ontogenetic scaling of the hindlimb muscles of the Greater Rhea (*Rhea*
681 *americana*). *Anatomia, Histologia, Embryologia*, published online.
682 Powell PL, Roy RR, Kanim P, Bello MA, and Edgerton VR. 1984. Predictability of skeletal muscle
683 tension from architectural determinations in guinea pig hindlimbs. *Journal of Applied*
684 *Physiology* 57:1715-1721.
685 Regnault S, Pitsillides AA, and Hutchinson JR. 2014. Structure, ontogeny and evolution of the patellar
686 tendon in emus (*Dromaius novaehollandiae*) and other palaeognath birds. *PeerJ PrePrints*
687 *2:e404v1*
688 R Development Core Team. 2010. R: A language and environment for statistical computing. Vienna,
689 Austria: R Foundation for Statistical computing.
690 Sacks RD, and Roy RR. 1982. Architecture of the hind limb muscles of cats: functional significance.
691 *Journal of Morphology* 173:185-195.
692 Schmidt-Nielsen K. 1984. *Scaling: Why is Animal Size so Important?* Cambridge University Press.
693 Shadwick RE. 1990. Elastic energy storage in tendons: Mechanical differences related to function and
694 age. *Journal of Applied Physiology* 68:1033-1040.
695 Smith N, Wilson A, Jespers K, and Payne R. 2006. Muscle architecture and functional anatomy of the
696 pelvic limb of the ostrich (*Struthio camelus*). *Journal of Anatomy* 209:765-779.
697 Smith NC, Jespers KJ, and Wilson A. 2010. Ontogenetic scaling of locomotor kinetics and kinematics
698 of the ostrich (*Struthio camelus*). *Journal of Experimental Biology* 213:1347-1355.
699 Smith NC, Payne RC, Jespers KJ, and Wilson AM. 2007. Muscle moment arms of pelvic limb muscles
700 of the ostrich (*Struthio camelus*). *Journal of Anatomy* 211:313-324.
701 Smith NC, and Wilson AM. 2013. Mechanical and energetic scaling relationships of running gait
702 through ontogeny in the ostrich (*Struthio camelus*). *Journal of Experimental Biology* 216:841-
703 849.
704 Taylor RC, Maloiy GMO, Weibel ER, Langman VA, Kamau JMZ, Seeherman HJ, and Heglund NC. 1981.
705 Design of the mammalian respiratory system. III. Scaling maximum aerobic capacity to body
706 mass: Wild and domestic mammals. *Respiration Physiology* 44:25-37.
707 Thorpe CT, Riley GP, Birch HL, Clegg PD, and Screen HR. 2014. Fascicles from energy-storing tendons
708 show an age-specific response to cyclic fatigue loading. *Journal of the Royal Society Interface*
709 11.

PeerJ PrePrints

710 Vanden Berge J, and Zweers G. 1993. Myologia. In: Baumel J, King A, Breazile J, Evans H, and Vanden
711 Berge J, eds. *Handbook of Avian Anatomy: Nomina Anatomica Avium*. Cambridge, MA:
712 Nuttall Ornithological Club, pp189-247.
713 Yoshikawa T, Mori S, Santiesteban AJ, Sun TC, Hafstad E, Chen J, and Burr DB. 1994. The effects of
714 muscle fatigue on bone strain. *Journal of Experimental Biology* 188:217-233.
715 Young JW. 2009. Ontogeny of joint mechanics in squirrel monkeys (*Saimiri boliviensis*): functional
716 implications for mammalian limb growth and locomotor development. *Journal of*
717 *Experimental Biology* 212:1576-1591.
718 Zinoviev A. 2006. Notes on the hind limb myology of the Ostrich (*Struthio camelus*). *Ornithologia*
719 33:53-62.

720

PeerJ PrePrints